# Optimally Designed BLDC Motor Equipped with Different Winding Layouts for Robotic Arms

Mohamed Y. Metwly, Landon Clark, Biyun Xie, JiangBiao He
Department of Electrical and Computer Engineering
University of Kentucky
Lexington, KY, USA
Email: mohamed.metwly@uky.edu

2023 IEEE Energy Conversion Congress and Exposition (ECCE) | 979-8-3503-1644-5/23/$31.00 ©2023 IEEE | DOI: 10.1109/ECCE53617.2023.10362061

***Abstract*—Robots have shown promising prospects in numerous applications, such as space exploration, disaster rescue, and nuclear waste remediation. Due to harsh environmental conditions, robotic arms are vulnerable to joint failures, especially the faults with joint motors and power electronic drives. Thus, optimal design of the employed motors is paramount to achieve a reliable and fault-tolerant robotic arm. The employment of brushless DC (BLDC) motors in robotic applications is of particular interest, not only for high reliability but also for high efficiency and high torque-producing capability. BLDC motors can be equipped with distributed and fractional-slot windings; however, fractional-slot concentrated winding (FSCW) outperforms distributed winding owing to their notable advantages, e.g., high slot fill factor, short-end turns, and low cogging torque. On the other hand, the resultant flux distribution is highly distorted. Therefore, this research presents the design optimization of BLDC motors with two fractional-slot windings, namely, non-overlapped 18-slot/16-pole and overlapped 18-slot/10-pole, based on the finite element methodology (FEM). Selected motors are first designed based on the sizing equations and further optimized using a multi-objective genetic algorithm (MOGA). Finally, a thorough performance comparison of the proposed winding configurations is conducted to highlight the optimal slot/pole combination for robotic applications.**

***Keywords*—Joint motors, machine design, winding layouts, collaborative robots**

## I. Introduction

Robots have been increasingly utilized in remote, hazardous, and safety-threatening environments owing to their enhanced safety, productivity, and flexibility [1-3]. In fact, the robot joint motors and their associated power electronic drives are prone to hardware failures due to the harsh environmental conditions [4, 5]. These failures may yield malfunction of the whole robotic arms and thus economic losses. Therefore, optimal design of the joint motors is crucial to enhance system reliability and further develop fault-tolerant methodology for the joint motors and drives [6].

The electric motors utilized in robotic arms constitute AC motors, brushed DC motors, brushless DC motors, servo motors, stepper motors, and DC linear actuators [7]. Servo motors exhibit high power density and high efficiency; thus, they are among the most commonly used motors in robotic applications [7]. However, high overall cost and complex control are the main disadvantages of servo motors. Stepper motor can be also considered for robotic arms due to the low cost and high starting torque; however, its main drawback is the dedicated control circuit, low power density, and high torque ripple [8]. For instance, a low-cost robotic manipulator with seven degrees-of-freedom (DOF) has been introduced using a stepper motor [8], while servo motors have been well operated in a 7-DOF robot arm [9]. Due to their high reliability, high torque-producing capability, and low maintenance cost, BLDC motors have been utilized intensively in robotic applications [10, 11]. The Kinova Gen3 robot arm adopts seven BLDC joint motors, as shown in Fig. 1. Therefore, a BLDC motor has been selected for investigation in this paper [12].

Despite the fact that many BLDC motors are configured with conventional distributed windings, recent designs explore fractional-slot concentrated windings (FSCW). The latter has notable merits over conventional winding layouts since it offers low cogging torque, short-end turns, and a high slot fill factor. Furthermore, FSCW-based permanent magnet (PM) machines provide outstanding advantages, including high efficiency, low cogging torque, and high torque density. On the contrary, space harmonics yield distorted air gap flux distribution, which constitutes the main drawback of FSCWs [13]. Moreover, eddy currents in the rotor core and PMs are included as a result of space harmonics and contribute to rotor losses [14].

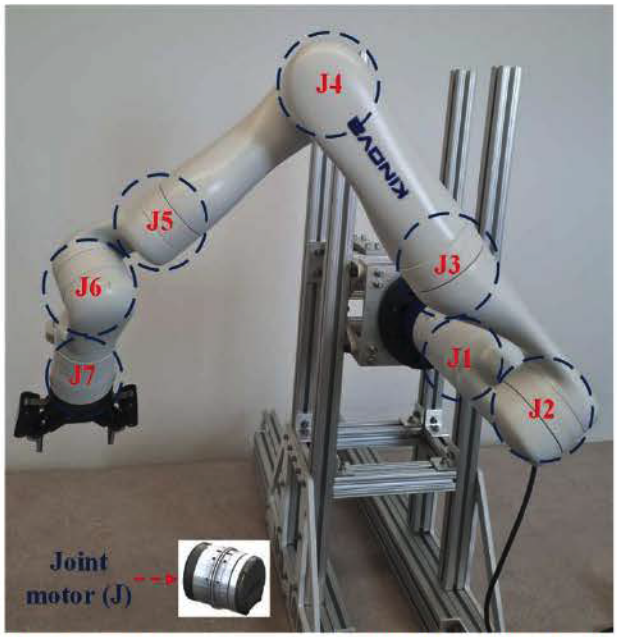


Fig. 1. Kinova Gen3 robotic arm with seven joint BLDC motors in the lab.

This material is based upon work supported by the U.S. National Science Foundation (NSF) under Grant No. 2205292.

 

Intensive research has been conducted aiming at reducing FSCW's eddy current losses, as well as the associated vibration and acoustic noise. For instance, the emerging stator shifting concept plays a key role in slot harmonics suppression [15, 16]. Several slot/pole combinations have been investigated in the literature, namely, 24-slot/10-pole [17] and 18-slot/10-pole [18], to demonstrate the efficacy of the stator shifting concept. These slot/pole combinations are overlapped windings with a coil pitch of two slots.

The main criteria when designing electric motors -besides cost- are the maximum torque density and minimum losses. Moreover, the motor's design parameters, such as the slot opening width and PM width to pole pitch ratio, have a substantial impact on the average output torque, torque ripple, and core losses [19]. Therefore, multi-objective optimization techniques have been proposed based on the finite element (FE) and analytical models [20]. FE models are more accurate than analytical ones; however, analytical models entail much lower computational burden.

The optimal design of the BLDC motors has been presented in the recent literature [10, 21]. In [10], the design of an electromagnetic actuator for robotic applications has been introduced using a three-phase BLDC motor. The initial design has been optimized based on the genetic algorithm (GA), considering the torque-to-weight and torque-to-inertia ratios as the optimization objectives. These objectives are crucial for the fast response in robotics. Furthermore, the optimal design of an interior permanent magnet (IPM) BLDC motor has been introduced to enhance the operation of the motor with low-resolution hall sensors [21].

In this paper, the design optimization of a BLDC motor for robotic arm joints is proposed using a three-phase surface-mounted permanent magnet (SPM) machine with fractional-slot windings. In this case, the non-overlapped FSCW 18-slot/16-pole is compared to the overlapped fractional-slot 18-slot/10-pole, considering the average torque, peak-to-peak torque ripple, core losses, and thermal behavior. The main contributions of this study are summarized as follows:

- BLDC motor design with possible slot/pole combinations, i.e., 18-slot/16-pole and 18-slot/10-pole, highlighting stator shifting concept.
- Multi-objective genetic algorithm (MOGA) optimization of the employed BLDC motor with the proposed winding layouts considering the above-mentioned performances.
- Comprehensive comparison between the fractional-slot winding configurations with various slot/pole combinations using the finite element analysis (FEA).

## II. Overall Design Optimization Methodology

In this study, three-phase SPM machines with two slot/pole combinations, namely, FSCW 18-slot/16-pole and fractional-slot 18-slot/10-pole, have been introduced. The 10-pole machine has been employed to test the stator shifting concept, in which the number of slots is doubled, and the number of poles remains constant. Fig. 2 depicts the proposed winding configurations, while their MMF harmonic spectra are shown in Fig. 3. The effect of the stator shifting on slot harmonic suppression is therefore highlighted since the torque-producing components for both layouts are shown in Fig. 3, while the dominant slot harmonic is omitted, i.e., the fourth harmonic ($h = 4$), when the 10-pole machine is employed. In this case, the 8th and the 5th harmonic components mainly contributed to the torque production for the 16-pole and 10-pole machines, respectively. Nevertheless, the induced rotor eddy current losses of the 16-pole machine are much higher than its 10-pole counterparts due to the inevitable slot harmonic, i.e., the 10th harmonic.

The proposed SPM-based BLDC motors with concentrated windings are first designed based on the sizing equations [22] and further optimized based on the FEA using a MOGA. In robotic applications, the average developed torque, torque ripple, and core losses are identified among the design optimization objectives to increase the robotic arm's payload, reduce vibration and noise in SPM machines, and prevent PM thermal demagnetization. The above-mentioned optimization performances cannot be concurrently achieved. Thus, the optimal trade-off between several optimization objectives is determined based on the proposed optimization model.

The main aim of the optimization algorithm is to minimize the following objective function, considering the magnet thickness $Y_m$, slot-opening ratio $t_{so}/\tau_{so}$, and PM arc $\alpha_{PM}$ as the decision variables, and the current density $J$ and slot fill factor $K_{cu}$ as the constraints. It is worth mentioning that the utilized cooling technique determines the current density, and the copper fill factor is chosen to optimize the number of effective machine winding turns and hence improve the torque density.

$$\underset{Y_m, \frac{t_{so}}{\tau_{so}}, \alpha_{PM}}{\text{minimize}} \quad F(X_i) \tag{1}$$

$$F(X_i) = \lambda_1 \frac{T'_{mean}}{T_{mean}(X_i)} + \lambda_2 \frac{T_{ripple}(X_i)}{T'_{ripple}} + \lambda_3 \frac{P_{core}(X_i)}{P'_{core}}$$

$$\text{Subject to} \quad \begin{matrix} J \le 4\ A/mm^2 \\ K_{cu} \le 0.4\ \% \\ T_{mean} \ge 1.52\ Nm \\ X_i^{min} \le X_i \le X_i^{max} \end{matrix} \tag{2}$$

where the average torque, torque ripple, and core losses are $T_{mean}(X_i)$, $T_{ripple}(X_i)$, and $P_{core}(X_i)$, respectively. Meanwhile, $T'_{mean}$, $T'_{ripple}$, and $P'_{core}$ are their initial values, respectively. $X_i^{min}$ and $X_i^{max}$ are the lower and upper boundaries of the design variables. Besides, $\lambda_1$, $\lambda_2$, and $\lambda_3$ are the weighting factors of the optimization objectives, respectively, whereas $\lambda_1 + \lambda_2 + \lambda_3 = 1$.

The optimization approach is highly affected by the selected weighting factors; however, there is no specific standard to define these factors [23]. In that study, it is supposed that the three selected objectives have different priorities. Thus, the weighting factors are determined such that $\lambda_1 = 0.4$, $\lambda_2 = 0.3$, and $\lambda_3 = 0.3$. The average torque production is undoubtedly the most crucial goal when designing the SPM machine. However, the performance of the SPM machine is substantially impacted by the torque ripple and core losses. The weighting factors are, therefore, determined.

The best trade-off between the three objectives was achieved at the optimal operating point, which was determined using a

MOGA-based optimization approach. The FE-based optimization results are shown in Fig. 4, in which $F(X_i)$ is referred to as the objective. It is clear that the objective function is minimized, and the optimal design is highlighted for both the 16-pole and 10-pole designs. Eventually, the motor design specifications and optimal parameters are revealed in Tables I and II, respectively.

TABLE I – BLDC MOTORS DESIGN SPECIFICATIONS

| | |
|---|---|
| Power (W) | 400 |
| Rated base speed (rpm) | 2500 |
| Rated torque (Nm) | 1.52 |
| DC link voltage | 48 |
| Electric loading (A/mm) | 12 |

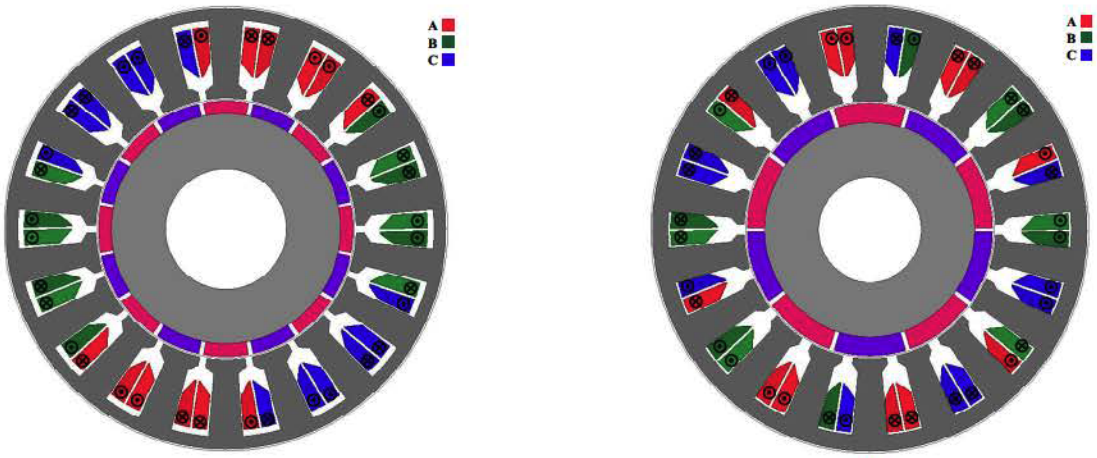


(a) (b)

Fig. 2. BLDC motor with various winding layouts (a) 18-slot/16-pole winding layout; (b) 18-slot/10-pole winding layout.

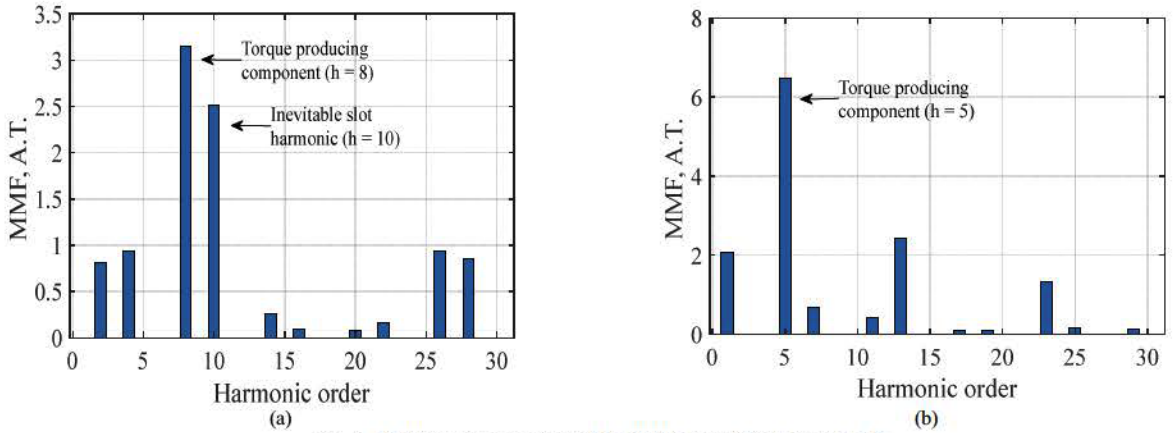


(a) (b)

Fig. 3. MMF harmonic spectra: (a) 18-slot/16-pole. (b) 18-slot/10-pole.

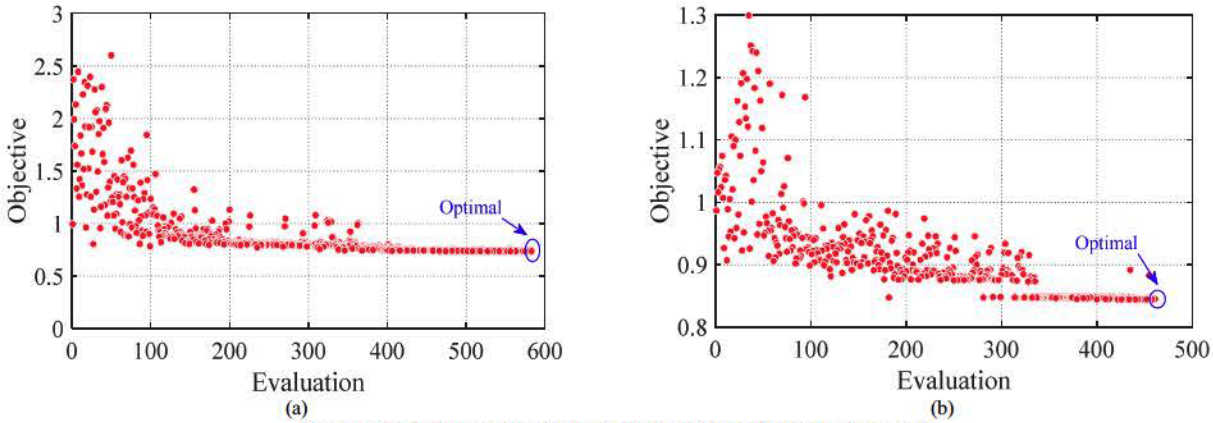


(a) (b)

Fig. 4. Optimization results using FEA: (a) 18-slot/16-pole. (b) 18-slot/10-pole.

TABLE II - THE BLDC MOTORS' MAIN PARAMETERS

| Slot/pole combination | 18-slot/ 16-pole | 18-slot/ 10-pole | Slot/pole combination | 18-slot/ 16-pole | 18-slot/ 10-pole |
|---|---|---|---|---|---|
| Stator outer diameter (mm) | 68.8 | | Magnet thickness (mm) | 2 | 2.2 |
| Stator inner diameter (mm) | 40.85 | 41.4 | Magnet arc ratio | 0.88 | 0.92 |
| Stack length (mm) | 62 | | No. of turns per coil | 7 | 9 |
| Air gap length (mm) | 0.5 | | Line current peak value (A) | 9.132 | 6.078 |
| Rotor diameter (mm) | 35.85 | 36 | Phase resistance (Ω) | 0.07335 | 0.1646 |
| Teeth width (mm) | 3.54 | 3.738 | Winding layer/coil pitch | Double layer/single | Double layer/two |
| Stator back iron height (mm) | 1.828 | 2.48 | | | |

## III. SIMULATION RESULTS

This research utilizes the ANSYS Motor-CAD to simulate the BLDC motor with the proposed winding layouts for robotic applications using the rated specifications in Table I. For a fair comparison, the same electric loading, outer diameter, and stack length have been used for both winding layouts. The two machines are simulated at the rated conditions, and their FEA results are given in Figs. 5 - 8. The flux density distributions of the employed machine with the two winding configurations are shown in Fig. 5. It is clear that the flux density in the tooth tips and rotor back iron is within the required value of 1.8 T for both winding layouts. This proves that the risk of magnetic saturation is alleviated, which further verifies the design optimization approach.

Fig. 6 shows the torque profiles of both the initial and optimal designs of the two winding layouts. For instance, for the 18-slot/10-pole, the average output torque of the optimal design is improved when compared to the initial one with 1.775 Nm and 1.57 Nm, respectively. Besides, the optimal 10-pole machine outperforms its 16-pole counterpart with higher average torque and lower torque ripple, i.e., the output torques are 1.775 Nm and 1.52 Nm, respectively. Both initial and optimal motors have the same back EMF profiles, as shown in Fig. 7. However, the 10-pole machine exhibits a higher voltage magnitude and thus a higher average torque when compared to the 16-pole one. It is proven from the back EMF profiles that the 3rd harmonic component is higher in the 10-pole machine than its 16-pole counterpart. Thus, it is recommended to employ the 18-slot/16-pole FSCW when the machine is fed by a sinewave modulated drive. However, the 18-slot/10-pole fractional-slot winding based on the stator shifting concept exhibits a better performance with the machines excited by square-wave modulated drives. Furthermore, a comprehensive comparison of the proposed winding layouts is revealed in Table III, highlighting the average output torque, rms back EMF, and core and PM losses. Thus, the 18-slot/10-pole combination has a better electromagnetic performance than the 18-slot/16-pole case.

Since the NdFeB magnets N38UH are used for the PMs, where the coercivity is 955 kA/m at the temperature of 20°C, the maximum magnetic field intensity is calculated to evaluate the demagnetization risk of the employed slot/pole combinations, as follows:

$$demag\_risk = \frac{H_{max}^{charg}}{H_c} \times 100 \quad (3)$$

where $H_{max}^{charg}$ and $H_c$ are the maximum magnetic field intensity and the coercivity of the N38UH PM, respectively. It is clear that the demagnetization risk is reduced when the 16-pole is employed, i.e., the demagnetization risk is 69.42% and 75.39% when the 16-pole and 10-pole machines are employed, respectively.

To further compare the proposed 18/16 and 18/10 slot/pole combinations, the temperature distribution is introduced since operating the electric motor at the proper temperature is crucial to enhance reliability. In PM machines, heat management is of particular interest since overheating may cause thermal demagnetization. In this paper, a preliminary thermal analysis of the SPM-based BLDC motor with the two selected winding configurations is carried out using the ANSYS Motor-CAD at different ambient temperatures, e.g., 20°C and 40°C. It is worth mentioning that natural cooling is adopted in this study. Iron, copper, and PM eddy current losses, listed in Table III, are the main sources of heat in the BLDC motor. The temperature distribution of the BLDC motor with the two winding layouts is revealed in Table IV. The two winding layouts are similar in thermal performance with a slightly improved behavior when the 16-pole machine is employed. For instance, the winding temperatures are 53.8°C and 57.4°C for the 16-pole and 10-pole machines, respectively. This is proved by the lower copper loss, listed in Table III. The same conclusion can be drawn at the two reference temperatures. As an illustrative example, the temperature distribution of the proposed winding layouts based on a simple transient thermal analysis is shown in Fig. 8 at an ambient temperature of 40°C.

TABLE III - QUANTITATIVE ANALYSIS OF THE SIMULATION RESULTS

| Output | 18-slot/16-pole | | 18-slot/10-pole | |
|---|---|---|---|---|
| | Initial | Optimal | Initial | Optimal |
| Average torque (Nm) | 1.419 | 1.52 | 1.57 | 1.775 |
| Peak-to-peak torque ripple (Nm) | 0.65 | 0.51 | 0.349 | 0.319 |
| Phase A back emf (V RMS) | 19.82 | 19.49 | 22.82 | 23.2 |
| Copper loss (W) | 13.33 | | 22.34 | |
| Stator core loss (W) | 17.25 | 15 | 14.86 | 13.54 |
| Rotor core loss (W) | 0.756 | 0.127 | 0.476 | 0.129 |
| PM loss (W) | 0.113 | 0.979 | 0.3 | 0.2 |

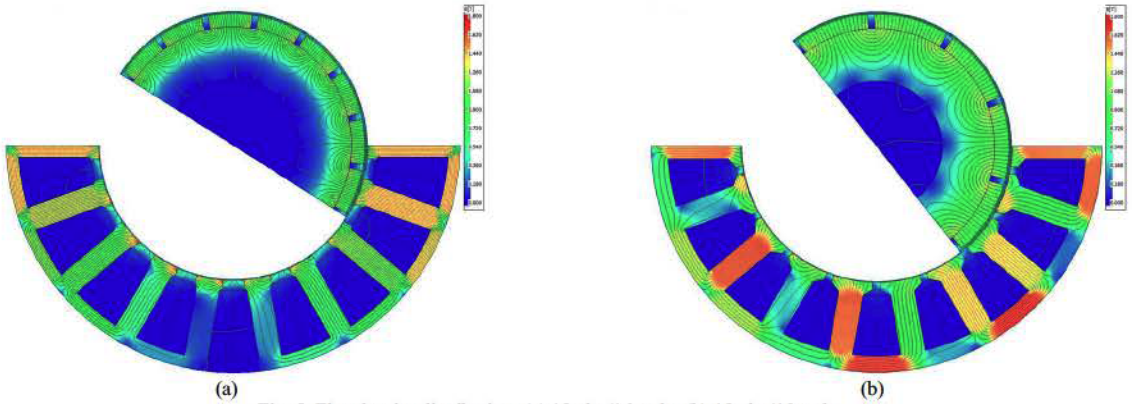

(a) (b)

Fig. 5. Flux density distribution: (a) 18-slot/16-pole. (b) 18-slot/10-pole.

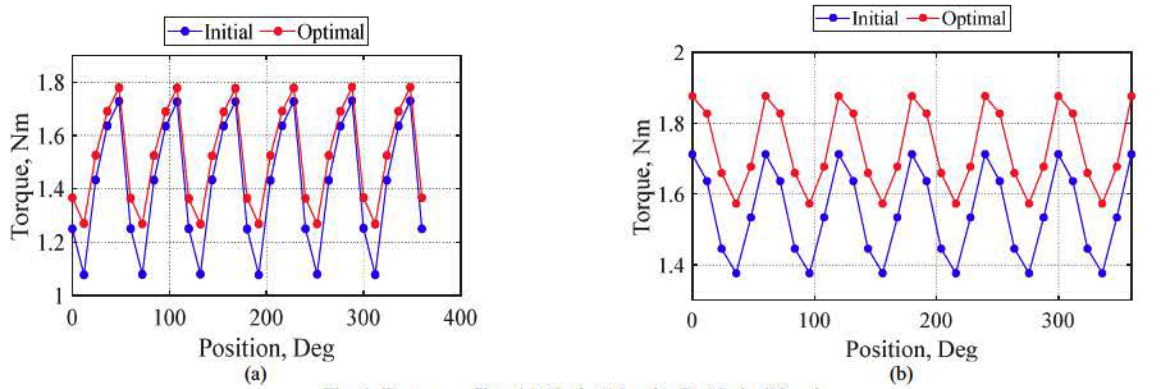


Fig. 6. Torque profiles: (a) 18-slot/16-pole. (b) 18-slot/10-pole.

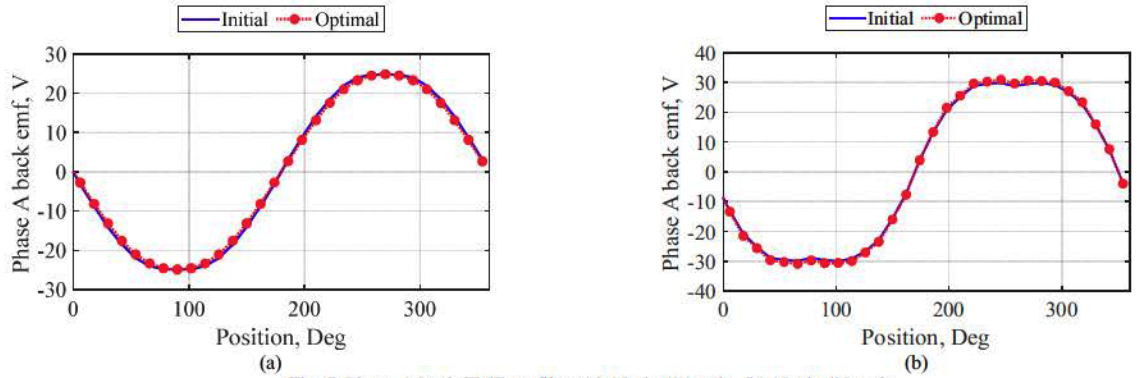


Fig. 7. Phase-A back EMF profiles: (a) 18-slot/16-pole. (b) 18-slot/10-pole.

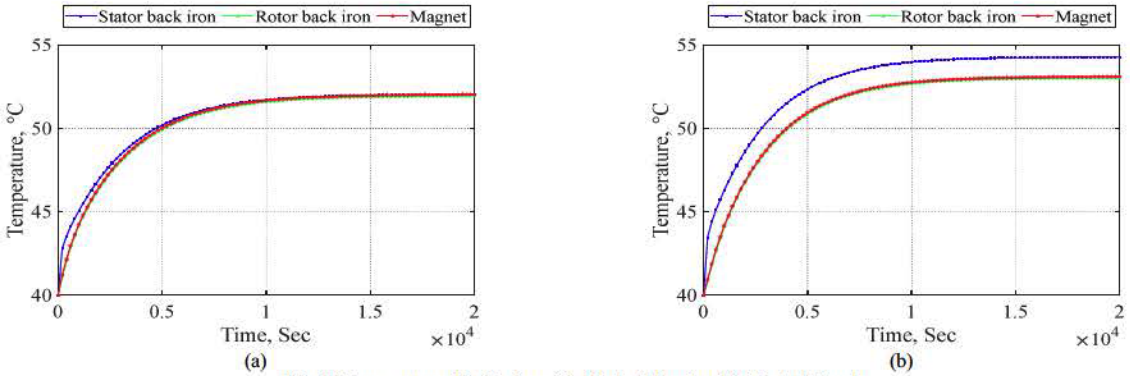


Fig. 8. Temperature distribution: (a) 18-slot/16-pole. (b) 18-slot/10-pole.

TABLE IV - TEMPERATURE DISTRIBUTION OF THE BLDC MOTOR WITH THE PROPOSED WINIDNG LAYOUTS

| Ambient Temp. | Winding [°C] | Stator back iron [°C] | Rotor back iron [°C] | Magnet [°C] |
|---|---|---|---|---|
| 18-slot/16-pole | | | | |
| 20°C | 34.7 | 32.9 | 32.7 | 32.8 |
| 40°C | 53.8 | 52 | 51.9 | 52 |
| 18-slot/10-pole | | | | |
| 20°C | 38.4 | 35.3 | 33.9 | 34 |
| 40°C | 57.4 | 53 | 54.3 | 53.1 |

## IV. CONCLUSION

This paper presents the performance analysis of an SPM-based BLDC motor for robotic arms when equipped with fractional-slot windings. The 18-slot/16-pole and 18-slot/10-pole configurations have been selected, which are designed based on the sizing equations and optimized by using the FEA. Both motors have the same performance from a flux density distribution perspective. However, the 10-pole machine exhibits better performance in terms of torque profiles. Moreover, stator core and PM losses are reduced when the 10-pole layout is employed, i.e., the stator core losses are 13.54 W and 15 W for the 10-pole and 16-pole machines, respectively.

Thermal and demagnetization analyses have been introduced to further compare the proposed winding configurations. The 16-pole machine shows a slightly lower demagnetization risk and exhibits almost similar thermal behavior when compared to its 10-pole counterpart. It can be concluded that the 18-slot/10-pole machine outperforms the 16-pole one for robotic applications, at which the machine is fed by a square-wave modulated drive. On the contrary, the 16-pole machine is more advantageous than the 10-pole one when the machine is energized by a sinewave modulated drive.

## REFERENCES


[1] Z. Mu, L. Han, W. Xu, B. Li, and B. Liang, "Kinematic analysis and fault-tolerant trajectory planning of space manipulator under a single joint failure," *Robotics and biomimetics,* vol. 3, no. 1, pp. 1-10, 2016.

[2] M. E. Moran, "Evolution of robotic arms," *Journal of robotic surgery,* vol. 1, no. 2, pp. 103-111, 2007.

[3] D. Zhu, Y. Ma, M. Wang, J. Yang, Y. Yin, and S. Liu, "LSO-FastSLAM: A New Algorithm to Improve the Accuracy of Localization and Mapping for Rescue Robots," *Sensors,* vol. 22, no. 3, p. 1297, 2022.

[4] G. Chen, L. Li, Y. Fu, B. Yuan, and J. Fei, "Halt Optimization Strategy for a Space Manipulator with a Joint-Locked Failure," *International Journal of Aerospace Engineering,* vol. 2020, 2020.

[5] V. K. Dalla and P. M. Pathak, "Power-optimized motion planning of reconfigured redundant space robot," *Proceedings of the Institution of Mechanical Engineers, Part I: Journal of Systems and Control Engineering,* vol. 233, no. 8, pp. 1030-1044, 2019.

[6] Z. Yin, N. Hu, J. Chen, Y. Yang, and G. Shen, "A review of fault diagnosis, prognosis and health management for aircraft electromechanical actuators," *IET Electric Power Applications,* vol. 16, no. 11, pp. 1249-1272, 2022.

[7] S. B. Niku, *Introduction to robotics: analysis, systems, applications*. Prentice hall New Jersey, 2001.

[8] M. Quigley, A. Asbeck, and A. Ng, "A low-cost compliant 7-DOF robotic manipulator," in *2011 IEEE International Conference on Robotics and Automation*, 2011: IEEE, pp. 6051-6058.

[9] A. Zhao, "Design of a brushless servomotor for a low-cost compliant robotic manipulator," *Master's thesis, EECS Department, University of California, Berkeley,* 2018.

[10] C. Hwang, P. L. Li, C.-T. Liu, and C. Chen, "Design and analysis of a brushless DC motor for applications in robotics," *IET electric power applications,* vol. 6, no. 7, pp. 385-389, 2012.

[11] S. Seok, A. Wang, D. Otten, and S. Kim, "Actuator design for high force proprioceptive control in fast legged locomotion," in *2012 IEEE/RSJ International Conference on Intelligent Robots and Systems*, 2012: IEEE, pp. 1970-1975.

[12] B. Xie and A. A. Maciejewski, "Maximizing the probability of task completion for redundant robots experiencing locked joint failures," *IEEE Transactions on Robotics,* vol. 38, no. 1, pp. 616-625, 2021.

[13] A. M. El-Refaie, "Fractional-slot concentrated-windings synchronous permanent magnet machines: Opportunities and challenges," *IEEE Transactions on industrial Electronics,* vol. 57, no. 1, pp. 107-121, 2009.

[14] E. Fornasiero, N. Bianchi, and S. Bolognani, "Slot harmonic impact on rotor losses in fractional-slot permanent-magnet machines," *IEEE Transactions on industrial electronics,* vol. 59, no. 6, pp. 2557-2564, 2011.

[15] A. S. Abdel-Khalik, S. Ahmed, and A. Massoud, "Application of stator shifting to five-phase fractional-slot concentrated winding interior permanent magnet synchronous machine," *IET Electric Power Applications,* vol. 10, no. 7, pp. 681-690, 2016.

[16] P. B. Reddy, K.-K. Huh, and A. M. El-Refaie, "Generalized approach of stator shifting in interior permanent-magnet machines equipped with fractional-slot concentrated windings," *IEEE Transactions on Industrial Electronics,* vol. 61, no. 9, pp. 5035-5046, 2014.

[17] A. S. Abdel-Khalik, S. Ahmed, and A. M. Massoud, "A six-phase 24-slot/10-pole permanent-magnet machine with low space harmonics for electric vehicle applications," *IEEE Transactions on Magnetics,* vol. 52, no. 6, pp. 1-10, 2016.

[18] K. Wang, Z. Zhu, G. Ombach, M. Koch, S. Zhang, and J. Xu, "Electromagnetic performance of an 18-slot/10-pole fractional-slot surface-mounted permanent-magnet machine," *IEEE Transactions on Industry Applications,* vol. 50, no. 6, pp. 3685-3696, 2014.

[19] D. Wang, X. Wang, and S.-Y. J. I. t. o. m. Jung, "Cogging torque minimization and torque ripple suppression in surface-mounted permanent magnet synchronous machines using different magnet widths," vol. 49, no. 5, pp. 2295-2298, 2013.

[20] D. Cao, W. Zhao, J. Ji, and Y. Wang, "Parametric equivalent magnetic network modeling approach for multiobjective optimization of PM machine," *IEEE Transactions on Industrial Electronics,* vol. 68, no. 8, pp. 6619-6629, 2020.

[21] H.-S. Seol, J. Lim, D.-W. Kang, J. S. Park, and J. Lee, "Optimal design strategy for improved operation of IPM BLDC motors with low-resolution hall sensors," *IEEE Transactions on Industrial Electronics,* vol. 64, no. 12, pp. 9758-9766, 2017.

[22] S. Huang, J. Luo, F. Leonardi, and T. A. J. I. T. o. I. A. Lipo, "A general approach to sizing and power density equations for comparison of electrical machines," vol. 34, no. 1, pp. 92-97, 1998.

[23] C. Ma and L. Qu, "Multiobjective optimization of switched reluctance motors based on design of experiments and particle swarm optimization," *IEEE Transactions on Energy Conversion,* vol. 30, no. 3, pp. 1144-1153, 2015.